

# Large quantum fluctuations in the strongly coupled spin-1/2 chains of green dioptase: a hidden message from birds and trees

O. Janson,\* A. A. Tsirlin, M. Schmitt, and H. Rosner†

*Max-Planck-Institut für Chemische Physik fester Stoffe, D-01187 Dresden, Germany*

(Dated: 22<sup>nd</sup> of April, 2010 — dedicated to Stefan-Ludwig Drechsler on the occasion of his 60<sup>th</sup> birthday)

The green mineral dioptase  $\text{Cu}_6\text{Si}_6\text{O}_{18}\cdot 6\text{H}_2\text{O}$  has been known since centuries and plays an important role in esoteric doctrines. In particular, the green dioptase is supposed to grant the skill to speak with trees and to understand the language of birds. Armed with natural samples of dioptase, we were able to unravel the magnetic nature of the mineral (presumably with hidden support from birds and trees) and show that strong quantum fluctuations can be realized in an essentially framework-type spin lattice of coupled chains, thus neither frustration nor low-dimensionality are prerequisites. We present a microscopic magnetic model for the green dioptase. Based on full-potential DFT calculations, we find two relevant couplings in this system: an antiferromagnetic coupling  $J_c$ , forming spiral chains along the hexagonal  $c$  axis, and an inter-chain ferromagnetic coupling  $J_d$  within structural  $\text{Cu}_2\text{O}_6$  dimers. To refine the  $J_c$  and  $J_d$  values and to confirm the proposed spin model, we perform quantum Monte-Carlo simulations for the dioptase spin lattice. The derived magnetic susceptibility, the magnetic ground state, and the sublattice magnetization are in remarkably good agreement with the experimental data. The refined model parameters are  $J_c=78$  K and  $J_d=-37$  K with  $J_d/J_c \simeq -0.5$ . Despite the apparent three-dimensional features of the spin lattice and the lack of frustration, strong quantum fluctuations in the system are evidenced by a broad maximum in the magnetic susceptibility, a reduced value of the Néel temperature  $T_N \simeq 15$  K  $\ll J_c$ , and a low value of the sublattice magnetization  $m=0.55 \mu_B$ . All these features should be ascribed to the low coordination number of 3 that outbalances the three-dimensional nature of the spin lattice.

PACS numbers: 71.20.Ps, 75.10.Pq, 75.30.Cr, 75.30.Et, 91.60.Pn

## I. INTRODUCTION

Since ancient times, emerald has been one of the most rare and treasured gemstones because of its bright and brilliant green color. However, by far not all gemstones that were collected as emeralds or varieties of it were indeed emeralds — many of them later appeared to be specimens of green dioptase (see Fig. 1). Nevertheless, this confusion contributed considerably to the assignment of many mysterious powers to this mineral, such as providing beauty, wealth and creativity. Especially, esoteric doctrines credit dioptase with the ability to grant the skill to speak with trees and understand the language of birds. Stimulated by such a rather complex realm of concealed powers, we attempt in the present study to unravel the also controversially debated magnetic properties based on the paradigm of quantum mechanics and modern electronic structure theory.

Dioptase is a copper silicate mineral forming remarkably large shiny green rhombohedral crystals. Scientifically, it was first described and named by René-Just Haüy in the famous "Traité de Minéralogie" in 1801.<sup>1</sup> Vauquelin, as reported in Ref. 1, found that dioptase was a copper mineral containing silicate and – erroneously – carbonate anions. Only later, pure dioptase samples were analyzed and recognized as copper silicate with crystal water.<sup>2</sup>

Structure determination showed that hydrous dioptase with the chemical composition  $\text{Cu}_6\text{Si}_6\text{O}_{18}\cdot 6\text{H}_2\text{O}$  is a cyclosilicate with 6-membered single rings of silica  $\text{Si}_6\text{O}_{18}$

(compare Fig. 1, left) crystallizing in the space group  $R\bar{3}$  (S. G. 148).<sup>3,4</sup> These rings are interconnected by  $\text{Cu}^{2+}$  ions with a characteristic local environment of elongated octahedra formed by oxygen atoms. The Cu–O bond length in this 4+2 arrangement is quite typical with about 1.96 Å for the distorted equatorial plane of the octahedra and a bit larger than usual (between 2.6 and 2.75 Å) for the apical oxygens belonging to the crystal water. Due to the sharing of the octahedral O–OH<sub>2</sub> edges, the magnetic  $\text{Cu}^{2+}$  ions form helical chains around the 3-fold axis along  $c$  (see Fig. 1). Thus, each Cu atom has two Cu neighbors along these chains and another Cu neighbor with which it forms an edge-shared  $\text{Cu}_2\text{O}_6$  dimer that connects two adjacent spiral chains (see Fig. 1).

The magnetic properties of green dioptase have been investigated in some experimental studies.<sup>4–8</sup> Although these studies yield quantitatively slightly varying results, likely also related to dioptase samples originating from different locations, they essentially converge in the description of dioptase as an antiferromagnet with a rather low Néel temperature ( $T_N \sim 15$  K) compared to the antiferromagnetic Curie-Weiss temperature of about 70 K. The ordered magnetic moment ( $m = 0.55\mu_B$ ) is drastically reduced with respect to the saturation moment of  $1 \mu_B$  for  $\text{Cu}^{2+}$ . Together with the broad maximum in the measured magnetic susceptibility,<sup>9</sup> this puts the compound in the family of spin 1/2 quantum magnets that can be described successfully in many cases by the isotropic Heisenberg model

$$\hat{H} = \sum_{\langle ij \rangle} J_{ij} \hat{S}_i \hat{S}_j, \quad (1)$$

at least for the low lying spin excitations. Here,  $J_{ij}$  represents the exchange interaction between spins located at the lattice sites  $i$  and  $j$ .

Although this model looks deceptively simple at the first glance, neither its solution for a seemingly ordinary situation nor the assignment of appropriate exchange integrals  $J_{ij}$  for a specific material are trivial in any way. It is obvious that the crystal structure of a compound is the key to understand its magnetic properties. On the other hand, an assignment of interaction parameters solely based on structural considerations can be completely misleading like in the case of  $(\text{VO})_2\text{P}_2\text{O}_7$ .<sup>10,11</sup> In recent years, even careful investigations based on accurate experimental data, but within a limited spectrum of methods, have suggested controversially discussed magnetic models for several compounds. A prominent example for this problem are the two closely related spin-1/2  $J_1$ - $J_2$  chain compounds  $\text{Li}_2\text{CuO}_2$  and  $\text{LiCu}_2\text{O}_2$ , for which consensus about their location in the magnetic phase diagram was established only recently.<sup>12–18</sup>

Thus, to establish the appropriate magnetic model for a new, complex material, the application of independent methods seems of crucial importance. In particular, the search for the relevant sector in the phase diagram can largely benefit from a detailed microscopic analysis based on modern band structure theory<sup>17,19–21</sup> in combination with numerical methods to solve subsequently the corresponding Heisenberg Hamiltonian, at least in an approximate way.<sup>22,23</sup>

In particular, for green diopside a magnetic model with antiferromagnetic (AFM) nearest-neighbor (NN) coupling  $J_c$  along the spiral chains (see Fig. 1, middle) and AFM coupling  $J_d$  within the structural  $\text{Cu}_2\text{O}_6$  dimers was suggested<sup>24</sup> on empirical grounds and evaluated using quantum Monte-Carlo simulations (QMC) to fit the experimental magnetic susceptibility. This study places the compound in proximity to a quantum critical point due to a competition between chain-like ordering along  $c$  and magnetic dimer formation caused by the AFM  $J_d$ . In contrast to Ref. 24, the results of our microscopic study place the compound in a different region of the phase diagram and assign the strong quantum fluctuations and the related magnetic properties to the small effective coordination number of the magnetic  $\text{Cu}^{2+}$  sites.

## II. METHODS

Electronic structure calculations were performed using the full potential non-orthogonal local-orbital minimum basis scheme `fplo9.00–33`.<sup>25</sup> For the scalar relativistic calculations within the local density approximation (LDA) the exchange and correlation potential of

Perdew and Wang was chosen. A well-converged  $k$ -mesh of  $8 \times 8 \times 8$  points was used for LDA calculations.<sup>26</sup> Wannier functions (WF) were calculated for the antibonding Cu  $3d_{x^2-y^2}$  states. Strong correlations are treated in a mean-field way within the LSDA+ $U$  approach.<sup>27</sup> For the double counting correction (DCC) we applied the two limiting cases: the around-mean-field (AMF) approach and the fully-localized limit (FLL).<sup>28</sup> The on-site Coulomb repulsion  $U_{3d}$  was varied within the physically reasonable ranges:  $U_{3d}=5.5\text{--}7.5$  eV for AMF and  $U_{3d}=6.5\text{--}9.5$  eV for FLL. The intra-atomic Hund's coupling  $J_{3d}$  was fixed to 1 eV. To allow for various spin ordering arrangements, the original hexagonal symmetry was reduced to the spacegroup  $P1$ . For the LSDA+ $U$  calculations, we used  $k$ -meshes of  $4 \times 4 \times 4$  points. The calculations were carefully checked for convergence. For the structural input, we used the crystal structure from Ref. 4.

Quantum Monte-Carlo (QMC) simulations were performed using the programs `looper` and `dirloop_sse` of the software package `ALPS`.<sup>29</sup> The magnetic susceptibility was simulated for  $N=10752$  sites clusters, containing 256 coupled chains of 42 sites each. In the temperature range  $T/J_c = 0.15\text{--}4.50$ , we used 25 000 sweeps for thermalization and 300 000 sweeps after thermalization. The resulting statistical errors ( $<0.1\%$ ) are far below the experimental inaccuracy. To evaluate the dependence of the static structure factor on the cluster size, we performed a series of simulations starting with a  $N=24$  sites cluster and consequently increasing it up to  $N=8232$  sites. Magnetization curves were simulated on  $N=1536$  sites clusters at  $T=0.025J_c$  using 50 000 sweeps for thermalization and 500 000 sweeps after thermalization. Statistical errors did not exceed 0.5%.

The experimental data were collected on a natural sample of green diopside. A green transparent crystal was mechanically detached from the calcite matrix and used for magnetic measurements without alignment in the magnetic field. The magnetic susceptibility was measured with a Quantum Design MPMS SQUID in the temperature range 2–380 K in applied fields up to 5 T.

## III. RESULTS

### A. Electronic structure and magnetic model

The electronic structure of the green diopside was calculated within the LDA. The atom-resolved density of states (DOS) is depicted in Fig. 2. The width of the valence band is about 10 eV, similar to other cuprates. States at the Fermi level evidence a metallic solution in contrast to the green transparent crystals indicating an insulating behavior. This well known shortcoming of the LDA approach originates from the underestimation of the strong Coulomb repulsion in the Cu  $3d$  shell. The insulating ground state can be restored by adding the missing part of correlation (i) via mapping onto a Hubbard model

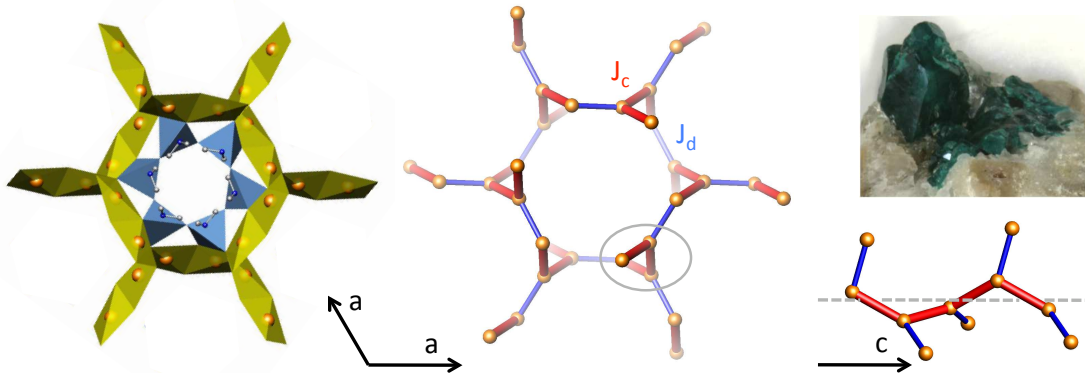


FIG. 1. (Color online) Left: Crystal structure of the green diopside. The  $\text{Cu}_2\text{O}_6$  dimers are shown in yellow and form a 3D network.  $\text{SiO}_4$  tetrahedra are shown blue. The crystal water is depicted by O (blue) and H (gray) atoms with O–H bonds. Middle: the magnetic model of the green diopside. Cu atoms are depicted as orange spheres, other atoms are not shown. The leading antiferromagnetic coupling  $J_c$  (red) forms spiral chains running along  $c$  perpendicular to the projection plane. The ferromagnetic coupling  $J_d$  (blue) within the structural  $\text{Cu}_2\text{O}_6$  dimers couples the chains into a three-dimensional framework. Right: section of the spiral chain along  $c$  (bottom) and a natural sample of green diopside grown on calcite (top).

or (ii) in a mean-field way by LSDA+ $U$  calculations. In this study, both approaches are used.

Despite the incorrect description of the ground state, LDA is known as a reliable tool for the evaluation of relevant orbitals and couplings. We start the analysis from the highest-lying states of the valence band. The well-separated band complex at the Fermi level is half filled and formed by antibonding Cu–O  $dp\sigma$  states. The energy range between  $-0.5$  and  $-2$  eV is dominated by non-bonding O and Cu states. At lower energies, around  $-2$  eV, states of the  $\text{SiO}_4$  tetrahedra and  $\text{H}_2\text{O}$  appear. The sizable  $\text{H}_2\text{O}$  contribution originates from the apical position of the crystal water in the distorted  $\text{CuO}_4(\text{H}_2\text{O})_2$  octahedra, and thus rather short Cu–O $_{\text{H}_2\text{O}}$  distances of 2.51 and 2.66 Å.

Typical for cuprates, the magnetic properties of the green diopside are ruled by the half-filled antibonding Cu–O  $dp\sigma$  band complex at the Fermi level. The width of this complex  $W$  can be used as a rough estimate for the leading couplings. Thus,  $W=0.8$  eV for the green diopside is comparable to related systems such as  $\text{Li}_2\text{ZrCuO}_4$  (buckled edge-shared chains,  $W=0.5$  eV),<sup>30</sup>  $\text{Cu}_2(\text{PO}_3)_2\text{CH}_2$  (distorted dimers,  $W=1$  eV)<sup>31</sup> or kapellasite (kagome lattice of corner-shared plaquettes with a Cu–O–Cu bond angle of about  $107^\circ$ ,  $W=0.9$  eV)<sup>22</sup>, but it is strongly reduced compared to  $\text{Sr}_2\text{CuO}_3$  (chains of corner-shared plaquettes,  $W=2.5$  eV)<sup>32</sup> or  $\text{SrCuO}_2$  (zigzag chains of edge-shared plaquettes,  $W=2$  eV)<sup>33</sup>. Based on such simplified comparative analysis, we can conjecture the leading couplings in diopside to be of the order of 100 K.

The orbitals which are relevant for the magnetism can be evaluated by a projection onto a set of local atomic orbitals. For each plaquette, one of the Cu–O bonds and a direction perpendicular to the plaquette are considered as local  $x$  and  $z$  coordinate axes, respectively. This way, we find that Cu states in the  $dp\sigma$  band complex have nearly

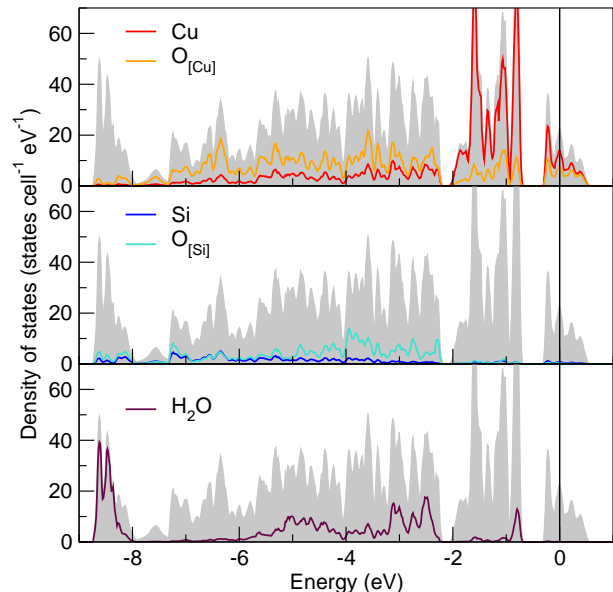


FIG. 2. (Color online) Total and atom-resolved LDA density of states for the green diopside. The antibonding Cu–O  $dp\sigma$  states form a well separated band complex at the Fermi level.

pure Cu  $3d_{x^2-y^2}$  character (see Fig. 3, right), although the plaquettes forming the structural  $\text{Cu}_2\text{O}_6$  dimers are considerably distorted. On contrary, the orbital-resolved DOS for the O states shows a mixture of  $2p_{x,y}$  and  $2p_z$  states. This mixing is caused by a non-coplanar arrangement of the neighboring dimers, sharing a common O atom.<sup>34</sup> Thus, although the O  $2p_z$  contributions are unusually high and seemingly hint at sizable O  $2p_\pi$  contributions, the states around the Fermi energy are clearly dominated by Cu–O  $dp\sigma$  states. Since the number of bands forming the band complex coincides with the num-

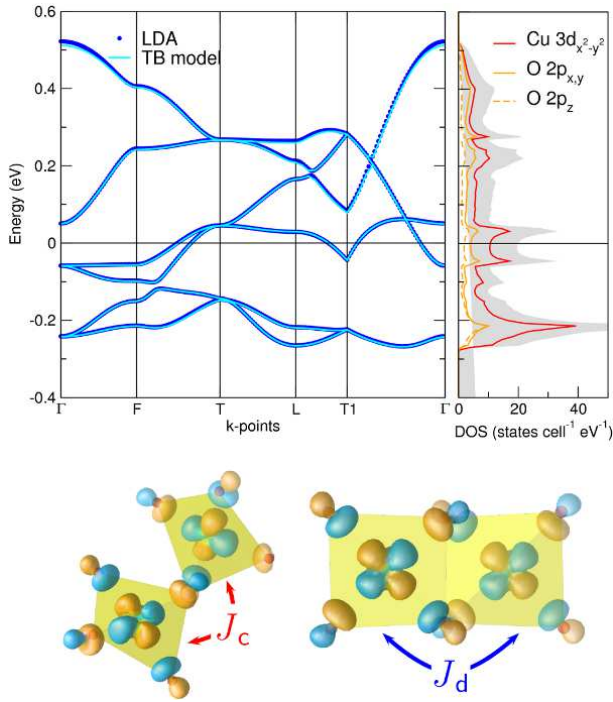


FIG. 3. (Color online) Top: Comparison of the antibonding  $dp\sigma$  bands from the LDA calculation and the tight-binding model (left) together with the orbital-resolved density of states (right). Bottom: Cu-centered Wannier functions superimposed upon the leading superexchange pathways.

ber of plaquettes in the unit cell, magnetic properties of the compound can be described by an effective one-band TB model.

In case of the green diopside, the evaluation of its magnetic model from simple geometric considerations based on the crystal structure only is difficult due to a complex 3D coupling of the structural dimers. To develop a magnetic model of the compound from microscopic grounds, the six bands forming the complex at the Fermi level were mapped onto an effective one-band TB model parameterized with transfer integrals  $t_{ij}$ . The Wannier function (WF) technique yields an unambiguous solution of this six-band problem. The resulting fit shows a nearly perfect description of the LDA band structure (Fig. 3).

Only two of the resulting transfer integrals  $t_{ij}$  are relevant:  $t_c = 126$  meV (the subscript  $c$  stands for “chain”), running along the spirals of dimers (in the  $c$  direction), and  $t_d = 104$  meV, the intra-dimer coupling (compare Fig. 1, middle). Other hoppings (except for the hopping  $t_{ic} = 24$  meV between the spirals) are smaller than 20 meV. To restore the insulating ground state, we map the TB model onto a Hubbard model considering an effective (one band) Coulomb repulsion  $U_{\text{eff}} = 4$  eV. For the strongly correlated limit at half-filling, both well justified for the green diopside, the lowest lying (magnetic) excitations can be efficiently described by a Heisenberg model. This way, the resulting magnetic exchange can

be derived using the second order perturbation theory expression  $J_{ij}^{\text{AFM}} = 4t_{ij}^2/U_{\text{eff}}$ . Since the original TB-model is a one-band model, only the antiferromagnetic contribution to the total magnetic exchange is accounted for in this approach. Thus, the resulting antiferromagnetic contributions for the leading couplings are  $J_c^{\text{AFM}} = 184$  K and  $J_d^{\text{AFM}} = 125$  K. Since exchange integrals  $J_{ij}^{\text{AFM}}$  are proportional to  $t_{ij}^2$ , all further exchanges are smaller than 7 K (less than 4% of the leading exchange) and can be neglected in first place.

Due to their close vicinity to  $90^\circ$  the intra-dimer Cu–O–Cu bond angle of  $97.4^\circ$  and inter-dimer angle of  $107.6^\circ$  require a careful estimation of the ferromagnetic contributions to the total exchange integrals, neglected in the effective one-band TB model approach presented above. Thus, we performed LSDA+ $U$  calculations of magnetic supercells with various collinear spin arrangements. The mapping of total energy differences onto a classical Heisenberg model results in an AFM exchange along the spirals chains  $J_c = 110$  K and a FM intra-dimer exchange  $J_d = -66$  K for a typical value of  $U_d = 6.5$  eV within the AMF DCC scheme.

In agreement with the expectations according to the Goodenough-Kanamori-Anderson rules,<sup>35–37</sup> the LSDA+ $U$  calculations evidence considerable FM contributions to both relevant exchange integrals  $J_c$  and  $J_d$ . In particular, the total value of  $J_c$  is strongly reduced compared to the estimate from the one-band model ( $J_c^{\text{AFM}} = 184$  K), yielding  $J_c^{\text{FM}} = -74$  K. For  $J_d$ , the closer proximity of the Cu–O–Cu angle to  $90^\circ$  leads to an even larger FM contribution  $J_d^{\text{FM}} = -191$  K which exceeds the AFM part  $J_d^{\text{AFM}}$ , resulting in a significantly FM total coupling  $J_d$  within the structural dimers.

Since the choice of DCC is non-trivial and can have a large impact on the resulting exchange parameters<sup>23,38</sup>, we compare the AMF results to FLL calculations. For the green diopside, we find that both DCC schemes yield similar results (Fig. 4). The only apparent difference is related to the values of  $U_{3d}$ : for FLL, about 2 eV larger  $U_{3d}$  values are required in order to obtain the same exchange integrals as AMF. The FM nature of  $J_d$  remains stable in the whole range of  $U_{3d}$  and for the two DCC schemes.

Although the qualitative microscopic model is well justified by varying the  $U_{3d}$  parameter in a rather wide range, the strong dependence of the resulting exchange integrals on  $U_{3d}$  impedes an accurate estimation of the absolute size and the ratio of the two couplings. In the next section, we refine the values of the exchange integrals by alternative methods.

To summarize the microscopic analysis, we obtain a model with two leading interactions: an AFM  $J_c$  running along the spiral (in the  $c$  direction) and an FM  $J_d$  inside structural  $\text{Cu}_2\text{O}_6$  dimers. We should note that a related magnetic model was proposed in Ref. 24. It is based on the same relevant exchange interactions, but implies an AFM intra-dimer coupling  $J_d$  in contrast to the FM nature of this coupling in our model. Remarkably, a model

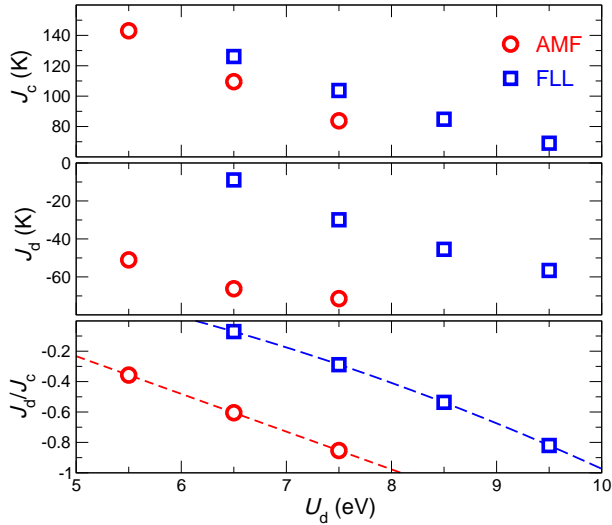


FIG. 4. (Color online) Results of total energy LSDA+ $U$  calculations: the leading exchange integrals ( $J_c$  and  $J_d$ ) and their ratio as a function of the on-site Coulomb repulsion  $U_{3d}$  for the around-mean field (AMF) and the fully localized limit (FLL) double counting correction schemes.

very similar to ours has been used to describe neutron scattering data for the dehydrated, black species of diophtase  $\text{Cu}_6\text{Si}_6\text{O}_{18}$ . This issue will be discussed in Sec. IV.

## B. Experimental results and model simulations

To challenge our model with respect to the experimental data, we measured the magnetic susceptibility of the green diophtase (Fig. 5) and used neutron diffraction results from previous studies.<sup>4</sup> Our susceptibility data are in good agreement with the earlier reports<sup>9,24</sup> and show a broad maximum at 50 K along with the magnetic ordering anomaly, evidenced by a kink at  $T_N \simeq 15$  K. We do not observe any appreciable field dependence up to 5 T. Above 200 K, the susceptibility can be fitted to the Curie-Weiss law, modified with an additional temperature-independent contribution  $\chi_0$ , responsible for core diamagnetism and van Vleck paramagnetism. The Curie-Weiss fit leads to  $\chi_0 = -7.2 \cdot 10^{-5}$  emu/mol, the effective magnetic moment  $\mu_{\text{eff}} = 1.99 \mu_B$  ( $g = 2.30$ ), and the Weiss temperature  $\theta = 43$  K. Note that the susceptibility below  $T_N$  depends on the crystal orientation in the magnetic field and can only be treated within an anisotropic model. In contrast, the magnetic behavior in the paramagnetic regime (above  $T_N$ ) is isotropic: the susceptibility simply scales due to different  $g$ -values along different crystal directions.<sup>39</sup> Since our microscopic study yields the exchange integrals of the isotropic (Heisenberg) Hamiltonian, we restrict ourselves to the data above  $T_N$ .

DFT calculations evidence two relevant interactions — the AFM intra-chain exchange  $J_c$  and the FM intra-dimer (inter-chain) exchange  $J_d$ . Below, we will com-

pare this model to the experimental results and refine the values of the leading exchange integrals. Since the microscopic model is well justified qualitatively (relevant couplings and their sign), its internal parameters  $J_c$  and  $J_d$  can be refined by varying them in a reasonable range and subsequently simulating the thermodynamical behavior for a given  $J_d/J_c$  ratio.

A method for simulations should be certainly consistent with the spin model. Since the two relevant couplings in diophtase form a non-frustrated, formally three-dimensional spin lattice, QMC simulations are natural and probably the only feasible choice. Therefore, we perform QMC simulations for the relevant parameter range  $-1 \leq J_d/J_c \leq -0.2$  of the  $J_c$ - $J_d$  model.

Simulations of the Heisenberg Hamiltonian yield a reduced magnetic susceptibility  $\chi^*$  which is related to the experimentally measured  $\chi$  by the expression:

$$\chi(T) = \frac{N_A g^2 \mu_B^2}{k_B J_c} \cdot \chi^* \left( \frac{T}{k_B J_c} \right) + \frac{C_{\text{imp}}}{T} + \chi_0, \quad (2)$$

where  $N_A$ ,  $k_B$  and  $\mu_B$  stand for the Avogadro constant, the Boltzmann constant and the Bohr magneton, respectively,  $g$  is the Lande factor,  $C_{\text{imp}}$  is the Curie constant to account for possible impurity and defect contributions and  $\chi_0$  is a temperature independent term, similar to the Curie-Weiss fit.

Although a fit to  $\chi(T)$  is commonly regarded as a sensitive probe for internal parameters of a magnetic model,<sup>40</sup> we find that the ratio  $J_d/J_c$  can be varied in a rather wide range ( $-0.8 \dots -0.4$ ) yielding a very good fit to the experimental data for the paramagnetic phase<sup>41</sup>. To improve our refinement of  $J_d/J_c$ , we have to address the magnetic ordering temperature  $T_N$ , which can be traced by a clear kink in the simulated curves. The reference to  $T_N$  yields  $J_d/J_c$  close to  $-0.5$ . The respective fit is shown in Fig. 5 (top). The resulting  $J_c = 78$  K agrees well with the DFT estimates: 110 K for  $U_{3d} = 6.5$  eV within the AMF scheme ( $J_d/J_c = -0.6$ ) and even better with 85 K yielded by  $U_{3d} = 8.5$  eV for the FLL scheme ( $J_d/J_c = -0.55$ ). Moreover,  $g = 2.26$  and  $\chi_0 = -6.9 \cdot 10^{-5}$  emu/mol are consistent with estimates from the Curie-Weiss fit (2.30 and  $-7.2 \cdot 10^{-5}$  emu/mol, respectively).

For a further test of our model, we will address its ground state properties. First, the propagation vector  $\vec{q}$  of the AFM ordered GS coincides with the experimentally observed  $\vec{q} = (0, 0, \frac{2}{3}\pi)$ <sup>4</sup> in the whole range  $-1 \leq J_d/J_c \leq -0.2$ . In this GS, the neighboring spins along the spiral chains ( $J_c$ ) align antiferromagnetically, while the ordering within the edge-sharing dimers ( $J_d$ ) is FM. This justifies the validity of our microscopic model, but does not allow for a more accurate refinement of the proposed value for the  $J_d/J_c$  ratio. For a further comparison, we use the sublattice magnetization ( $m$ ) that has been previously estimated in neutron diffraction experiments and amounts to  $0.55 \mu_B$ .<sup>4</sup>

Unfortunately, the theoretical estimation of  $m$  is not straightforward for two reasons. First, the simulations

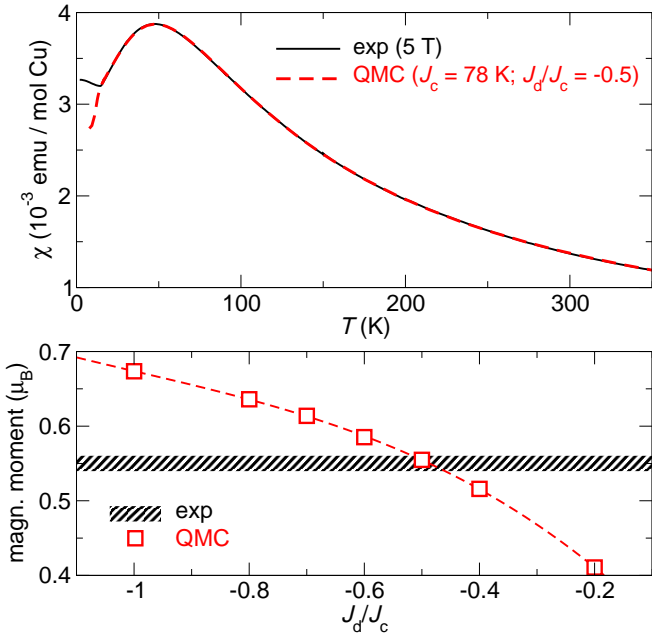


FIG. 5. (Color online) Top: The quantum Monte-Carlo (QMC) fit to the experimental magnetic susceptibility (per mol Cu). Bottom: QMC results for the ordered magnetic (sublattice) moment as a function of the  $J_d/J_c$  ratio. The experimental value from neutron diffraction<sup>4</sup> with an error bar is depicted by a striped bar.

do not yield the magnetic moment in the ordered state directly. Instead, it can be estimated based on the static structure factor or on spin correlations. Second, 3D coupling is crucial for the magnetic ordering of the green dioptase, thus sizable finite size effects are expected even for rather large clusters. To account for these effects, we use the general procedure from Ref. 42 and estimate the magnetic moment  $m$  based on a finite-size scaling of the static structure factor, taken for the propagation vector of the ordered structure. The results of simulations for various  $J_d/J_c$  ratios are shown in Fig 5 (bottom). Remarkably, the theoretical  $m$  for  $J_d/J_c = -0.5$  is in good agreement with the experimental value.

Finally, we can introduce a magnetic field term to our Hamiltonian and simulate the behaviour of magnetization  $M$  as a function of the reduced magnetic field  $0 \leq h^* \leq 5J_d$ . Such a simulation could be an additional test for our model, since high-field magnetization experiments were recently announced.<sup>9</sup> Therefore, we simulate  $M(h^*)$  curves for  $J_d/J_c = -0.5 \pm 0.2$  and scale them using the expression

$$M(h) = M\left(\frac{k_B J_c}{g \mu_B} h^*\right), \quad (3)$$

adopting the  $J_c$  and  $g$  values from the fits to  $\chi(T)$ . The resulting curves shown in Fig. 6 have similar shape and only slightly different values of the saturation field.<sup>43</sup> Therefore, the experimental  $M(h)$  dependence is unlikely

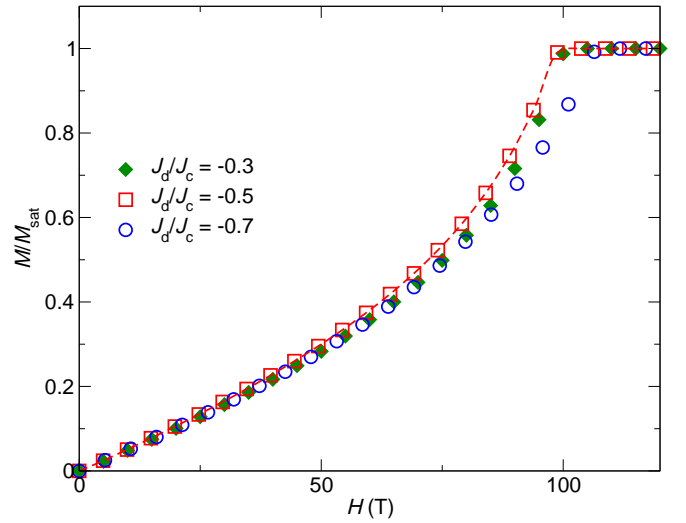


FIG. 6. (Color online) Simulated high field magnetization curves for three different values of the  $J_d/J_c$  ratio. The magnetic field is scaled by adopting the values of  $J_c$  and  $g$  from the fits to  $\chi(T)$ .

to facilitate a further refinement of the model parameters due to practical resolution limits at high magnetic fields. In addition, the predicted value of the saturation field remains challenging for present-day experimental facilities.

#### IV. DISCUSSION

In our model, the spin lattice of the green dioptase comprises AFM couplings  $J_c$  between the corner-sharing  $\text{CuO}_4$  plaquettes and FM couplings  $J_d$  between the edge-sharing plaquettes (Fig. 1). This situation is not surprising, because the corner-sharing connection normally leads to  $180^\circ$  superexchange, while the edge-sharing connection corresponds to the Cu–O–Cu angle close to  $90^\circ$ . However, the crystal structure of the green dioptase shows a tiny difference between the superexchange pathways. The twisted configuration of the corner-sharing plaquettes leads to the Cu–O–Cu angle of  $107.6^\circ$  for  $J_c$  that is substantially larger than  $97.4^\circ$  for  $J_d$ . The smaller angle for  $J_d$  still fits to the general trend, predicted by Goodenough-Kanamori-Anderson rules.<sup>35–37</sup> On the other hand, the green dioptase is very close to the “critical regime” of the Cu–O–Cu superexchange. Then, even a weak structural change could lead to a strong modification of the exchange couplings, making an empirical assignment of the parameter region difficult. For example, the earlier theoretical analysis assumed AFM coupling for both  $J_c$  and  $J_d$ .<sup>24</sup> Therefore, we used a quantitative microscopic approach and demonstrated that this empirical assumption is not consistent with the electronic structure of the compound.

To examine whether small changes in the crystal structure may lead to a modification of the microscopic model, the consideration of structurally closely related

compounds is a natural approach. The dehydration transforms the green dioptase into the black dioptase  $\text{Cu}_6\text{Si}_6\text{O}_{18}$  that essentially keeps the 3D framework-type crystal structure (Fig. 1) but lacks water molecules. The Cu–O–Cu angles amount to  $110.7^\circ$  and  $97.3^\circ$  for  $J_c$  and  $J_d$ , respectively.<sup>44</sup> Thus, based on basic structural arguments, the signs of the two couplings should persist, while the absolute values are likely increased. This prediction is in line with the experimental data, indicating a large Weiss temperature  $\theta$  of 180 K<sup>7</sup> of the black dioptase compared to  $\theta=43$  K in the green dioptase (Sec. III B). In addition, neutron diffraction studies evidence similar magnetic structures for the black and green dioptase.<sup>7</sup> On the other hand, a very recent study of black dioptase based on extended Hückel calculations and a 1D fit to the magnetic susceptibility assigns the compound to the model family of AFM chain compounds with very weak interchain interactions.<sup>45</sup>

Further examples of the dioptase structure are given by the hydrated and anhydrous Cu germanates  $\text{Cu}_6\text{Ge}_6\text{O}_{18} \cdot x\text{H}_2\text{O}$  with  $x = 0$  and 6. These compounds were previously considered as coupled frustrated spin chains, because a sizable next-nearest-neighbor coupling along the spiral chains was assumed.<sup>46,47</sup> This assumption is rather empirical and mainly motivated by the chemical similarity to the well-known spin-Peierls compound  $\text{CuGeO}_3$  with its frustrated spin chains of edge-sharing  $\text{CuO}_4$  plaquettes.<sup>48</sup> However, the pronounced difference in the crystal structures strongly impedes a reliable transfer of the well established magnetic model of the chain compound  $\text{CuGeO}_3$  to the Ge-dioptase  $\text{Cu}_6\text{Ge}_6\text{O}_{18}$ .<sup>46</sup> Based on the results for the Si-dioptase, we would expect sizable AFM  $J_c$ , while  $J_d$  is either FM or AFM. In the case that the FM and AFM contributions to  $J_d$  are close to cancel each other, the inter-chain coupling is effectively switched off, and long-range couplings along the spiral chains could alter the physics. The above empirical analysis gives no clear evidence for significant long-range couplings, but further microscopic studies should challenge this conclusion. Thus, since the minor structural changes in the dioptase family might be crucial for changes in the leading magnetic couplings and the understanding of their magnetic properties, a detailed comparative study is underway.<sup>49</sup>

Taking the green dioptase as an example, we have derived the basic features of the dioptase spin lattice. This spin lattice is unfrustrated, hence we should preclude any references to the frustrated spin chain model, at least for the green dioptase  $\text{Cu}_6\text{Si}_6\text{O}_{18} \cdot 6\text{H}_2\text{O}$ . It is worth to mention that the dioptase structure does *not* give rise to the star lattice (decorated honeycomb lattice), as it may seem on the first glance.<sup>50</sup> Such confusion could arise from a specific projection of the crystal structure, where the spiral chains look like flat frustrated triangles (compare to the middle panel of Fig. 1).

After shortly outlining what the dioptase spin lattice is not, it is more important to establish what it actually is: uniform AFM spin chains aligned along the  $c$  direction

are arranged on the honeycomb lattice, i.e., each chain is coupled to three neighboring chains, and the system is geometrically 3D (Fig. 1). However, the *total* coordination number is as low as three: each atom has two  $J_c$  bonds and one  $J_d$  bond only. Thus, the couplings in the  $ab$  plane form a kind of a “sparse” honeycomb lattice. The reduction in the coordination number has strong effect on the magnetic properties.

Experimental data for the green dioptase evidence strong quantum fluctuations: the broad susceptibility maximum at  $T_{\text{max}}^x/J_c \simeq 0.64$ , the low Néel temperature ( $T_N/J_c \simeq 0.2$ ), and the reduced sublattice magnetization ( $0.55 \mu_B$  compared to  $1 \mu_B$  for the classical spin- $\frac{1}{2}$  systems). Strong quantum fluctuations are usually observed in low-dimensional and/or frustrated spin systems. For example, the archetypal two-dimensional spin model of the square lattice reveals the susceptibility maximum at  $T_{\text{max}}^x/J \simeq 1.0$  and a sublattice magnetization of  $0.6 \mu_B$ .<sup>42</sup> To reduce the ordering temperature down to  $T_N/J = 0.2$ , a very weak interlayer coupling  $J_\perp/J \sim 10^{-4}$  is required.<sup>51</sup> Thus, the quantum fluctuations in the dioptase spin lattice are even stronger than in the square lattice, despite the 3D geometry.

Quantum fluctuations in a 3D spin system can arise from the magnetic frustration (see Ref. 52 for an instructive example). However, *the dioptase spin lattice is neither low-dimensional, nor frustrated*, hence its quantum behavior has a different origin. We suggest that the long-range magnetic ordering in dioptase is impeded by the low coordination number of the lattice, because the low number of bonds reduces the exchange energy that should stabilize the ordered ground state. The dioptase lattice can thus be compared to low-dimensional spin systems with similar coordination numbers. For example, the honeycomb lattice having three bonds per site reveals the low sublattice magnetization of  $0.54 \mu_B$  and  $T_{\text{max}}^x/J \simeq 0.7$  (compare to  $0.6 \mu_B$  and 1.0 for the square lattice with four bonds per site).<sup>53</sup> The apparent similarity between the dioptase and the honeycomb lattice clearly shows that the coordination number is the actual criterion of the “low-dimensionality”, as long as the magnitude of quantum fluctuations (the tendency towards the quantum behavior) is considered. Although the conclusion is a natural consequence of simple energy considerations, this is often overlooked. While neither the dioptase crystal structure, nor its spin model look low-dimensional, the essential physics is governed by strong quantum fluctuations, typical for low-dimensional magnets. The above considerations should stimulate further studies of dioptase-structure materials and the respective spin model.

## V. SUMMARY AND OUTLOOK

Based on density functional calculations, quantum Monte-Carlo simulations and magnetic measurements we have derived a new magnetic model for the natural min-

eral green diopside  $\text{Cu}_6\text{Si}_6\text{O}_{18}\cdot 6\text{H}_2\text{O}$  on a microscopic basis. We have shown that green diopside can be well described by a quantum spin  $1/2$  Heisenberg model with essentially two relevant interactions: an NN AFM intra-chain coupling  $J_c \sim 78\text{K}$  within the spiral chains running along the crystallographic  $c$  direction, and a NN FM intra-dimer (inter-chain) coupling  $J_d \sim -37\text{K}$  within the structural  $\text{Cu}_2\text{O}_6$  dimers. The calculated temperature dependence of the magnetic susceptibility, the magnetic ground state, the ordering temperature and the sublattice magnetization for the suggested model parameters are in very good agreement with the experimental data. From our results we conclude that the diopside spin lattice is neither low-dimensional nor frustrated, but exhibits large quantum fluctuations due to a small effective coordination number of its magnetic sites despite the three-dimensional lattice geometry.

Our approach demonstrates the great potential of the combination of modern band structure methods and numerical simulations with magnetic measurements for a

reliable modeling of the magnetic properties for complex compounds. An empirically based assignment of interaction parameters for structurally complex systems can be easily misleading and restrict studies to inappropriate regions of the magnetic phase diagram.<sup>24</sup> Since minor structural changes may cause drastic changes in the leading magnetic couplings, especially for couplings via bonds close to  $90^\circ$  relevant in the diopside family, a detailed comparative study for the hydrous and anhydrous Si- and Ge-diopside compounds is in progress.<sup>49</sup>

## ACKNOWLEDGMENTS

We are grateful to Deepa Kasinathan for enlightening discussions, Marcus Schmidt for providing us with the samples of diopside and Walter Schnelle for supporting the thermodynamical measurements and valuable comments. A. Ts. was supported by the postdoctoral fellowship of the Alexander von Humboldt foundation.

- 
- \* janson@cpfs.mpg.de  
† rosner@cpfs.mpg.de
- <sup>1</sup> R. J. Haiiy, *Traité de Minéralogie*, Vol. 3 (Paris, 1801) pp. 136–141.
  - <sup>2</sup> H. Hess, *Ann. Phys. (Leipzig)* **16**, 360 (1829).
  - <sup>3</sup> H. G. Heide and K. Boll-Dornberger, *Acta Crystallogr.* **8**, 425 (1955).
  - <sup>4</sup> E. L. Belokoneva, Y. K. Gubina, J. B. Forsyth, and P. J. Brown, *Phys. Chem. Minerals* **29**, 430 (2002).
  - <sup>5</sup> R. D. Spence and J. H. Muller, *J. Chem. Phys.* **29**, 961 (1958).
  - <sup>6</sup> R. E. Newnham and R. P. Santoro, *Phys. Status Solidi* **19**, K87 (1967).
  - <sup>7</sup> M. Wintenberger, G. André, and M. F. Gardette, *Solid State Comm.* **87**, 309 (1993).
  - <sup>8</sup> I. A. Kiseleva, L. P. Ogorodova, L. V. Melchakova, and M. R. Bisengalieva, *J. Chem. Thermodyn.* **25**, 621 (1993).
  - <sup>9</sup> H. Ohta, S. Okubo, N. Souda, M. Tomoo, T. Sakurai, T. Yoshida, E. Ohmichi, M. Fujisawa, H. Tanaka, and R. Kato, *Appl. Magn. Reson.* **35**, 399 (2009).
  - <sup>10</sup> D. C. Johnston, J. W. Johnson, D. P. Goshorn, and A. J. Jacobson, *Phys. Rev. B* **35**, 219 (1987).
  - <sup>11</sup> A. W. Garrett, S. E. Nagler, D. A. Tennant, B. C. Sales, and T. Barnes, *Phys. Rev. Lett.* **79**, 745 (1997); arXiv:cond-mat/9704092.
  - <sup>12</sup> M. Boehm, S. Coad, B. Roessli, A. Zheludev, M. Zolliker, P. Böni, D. M. Paul, H. Eisaki, N. Motoyama, and S. Uchida, *Europhys. Lett.* **43**, 77 (1998).
  - <sup>13</sup> W. E. A. Lorenz, R. O. Kuzian, S.-L. Drechsler, W.-D. Stein, N. Wizen, G. Behr, J. Málek, U. Nitzsche, H. Rosner, A. Hiess, W. Schmidt, R. Klingeler, M. Loewenhaupt, and B. Büchner, *Europhys. Lett.* **88**, 37002 (2009); arXiv:0909.5687.
  - <sup>14</sup> T. Masuda, A. Zheludev, A. Bush, M. Markina, and A. Vasiliev, *Phys. Rev. Lett.* **92**, 177201 (2004); arXiv:cond-mat/0310126.
  - <sup>15</sup> S.-L. Drechsler, J. Málek, J. Richter, A. S. Moskvin, A. A. Gippius, and H. Rosner, *Phys. Rev. Lett.* **94**, 039705 (2005); arXiv:cond-mat/0411418.
  - <sup>16</sup> T. Masuda, A. Zheludev, A. Bush, M. Markina, and A. Vasiliev, *Phys. Rev. Lett.* **94**, 039706 (2005); arXiv:cond-mat/0412245.
  - <sup>17</sup> A. A. Gippius, E. N. Morozova, A. S. Moskvin, A. V. Zalessky, A. A. Bush, M. Baenitz, H. Rosner, and S.-L. Drechsler, *Phys. Rev. B* **70**, 020406 (2004); arXiv:cond-mat/0312706.
  - <sup>18</sup> T. Masuda, A. Zheludev, B. Roessli, A. Bush, M. Markina, and A. Vasiliev, *Phys. Rev. B* **72**, 014405 (2005); arXiv:cond-mat/0412625.
  - <sup>19</sup> H. Rosner, R. R. P. Singh, W. H. Zheng, J. Oitmaa, S.-L. Drechsler, and W. E. Pickett, *Phys. Rev. Lett.* **88**, 186405 (2002); arXiv:cond-mat/0110003.
  - <sup>20</sup> A. A. Tsirlin and H. Rosner, *Phys. Rev. B* **79**, 214416 (2009); arXiv:0901.0154.
  - <sup>21</sup> A. A. Tsirlin, A. M. Abakumov, G. van Tendeloo, and H. Rosner, unpublished.
  - <sup>22</sup> O. Janson, J. Richter, and H. Rosner, *Phys. Rev. Lett.* **101**, 106403 (2008); arXiv:0806.1592.
  - <sup>23</sup> O. Janson, J. Richter, P. Sindzingre, and H. Rosner unpublished; arXiv:1004.2185.
  - <sup>24</sup> C. Gros, P. Lemmens, K.-Y. Choi, G. Güntherodt, M. Baenitz, and H. H. Otto, *Europhys. Lett.* **60**, 276 (2002); arXiv:cond-mat/0208106.
  - <sup>25</sup> K. Koepf and H. Eschrig, *Phys. Rev. B* **59**, 1743 (1999); fplo.de.
  - <sup>26</sup> J. P. Perdew and Y. Wang, *Phys. Rev. B* **45**, 13244 (1992).
  - <sup>27</sup> H. Eschrig, K. Koepf, and I. Chaplygin, *J. Solid State Chem.* **176**, 482 (2003); arXiv:cond-mat/0301558.
  - <sup>28</sup> M. T. Czyżyk and G. A. Sawatzky, *Phys. Rev. B* **49**, 14211 (1994).
  - <sup>29</sup> A. Albuquerque, F. Alet, P. Corboz, P. Dayal, A. Feiguin, S. Fuchs, L. Gamper, E. Gull, S. Grtler, A. Honecker, R. Igarashi, M. Körner, A. Kozhevnikov, A. Läuchli,



- S. Manmana, M. Matsumoto, I. McCulloch, F. Michel, R. Noack, G. Pawłowski, L. Pollet, T. Pruschke, U. Schollwöck, S. Todo, S. Trebst, M. Troyer, P. Werner, and S. Wessel, *J. Magn. Magn. Mater.* **310**, 1187 (2007); arXiv:0801.1765; alps.comp-phys.org.
- <sup>30</sup> M. Schmitt, J. Málek, S.-L. Drechsler, and H. Rosner, *Phys. Rev. B* **80**, 205111 (2009); arXiv:0911.0307.
- <sup>31</sup> M. Schmitt, A. A. Gippius, K. S. Okhotnikov, W. Schnelle, K. Koch, O. Janson, W. Liu, Y.-H. Huang, Y. Skourski, F. Weickert, M. Baenitz, and H. Rosner, *Phys. Rev. B* **81**, 104416 (2010).
- <sup>32</sup> H. Rosner, H. Eschrig, R. Hayn, S.-L. Drechsler, and J. Málek, *Phys. Rev. B* **56**, 3402 (1997); arXiv:cond-mat/9704210.
- <sup>33</sup> N. Nagasako, T. Oguchi, H. Fujisawa, O. Akaki, T. Yokoya, T. Takahashi, M. Tanaka, M. Hasegawa, and H. Takei, *J. Phys. Soc. Jpn.* **66**, 1756 (1997).
- <sup>34</sup> To prove that, we plotted the orbital-resolved DOS for individual atoms. The states corresponding to the O atoms bridging two Cu atoms in a dimer show a clearly planar character. For the O atoms linking two neighboring dimers, the contributions from O  $2p_x$  and O  $2p_z$  are comparable, because the O  $2p_z$  states correspond to the O  $2p_x$  states of the neighbor-dimer, while the states from O  $2p_y$  are negligible.
- <sup>35</sup> J. B. Goodenough, *Phys. Rev.* **100**, 564 (1955).
- <sup>36</sup> J. Kanamori, *J. Phys. Chem. Solids* **10**, 87 (1959).
- <sup>37</sup> P. W. Anderson, *Phys. Rev.* **79**, 350 (1950).
- <sup>38</sup> A. A. Tsirlin and H. Rosner, unpublished.
- <sup>39</sup> O. Janson, W. Schnelle, M. Schmidt, Y. Prots, S.-L. Drechsler, S. K. Filatov, and H. Rosner, *New J. Phys.* **11**, 113034 (2009); arXiv:0907.4874.
- <sup>40</sup> We should note, that a good fit to the experimental magnetic susceptibility is by no means an evidence that the model itself is correct, since essentially different sets of parameters for the same spin lattice and even for different lattices can yield similar macroscopic magnetic behavior.
- <sup>41</sup> For the ordered phase, anisotropy plays a crucial role. Since the simulated model is isotropic, the temperature range corresponding to the AFM ordered phase (below  $T_N < 15$  K) was excluded from the fit.
- <sup>42</sup> A. W. Sandvik, *Phys. Rev. B* **56**, 11678 (1997); arXiv:cond-mat/9707123.
- <sup>43</sup> For non-frustrated spin lattice in diopside, the value of the saturation field depends on  $J_c$  and  $g$ , but is not affected by the  $J_d/J_c$  ratio in case of a FM  $J_d$ .
- <sup>44</sup> K. H. Breuer, W. Eysel, and R. Mueller, *Z. Krist.* **187**, 15 (1989).
- <sup>45</sup> J. Law, C. Hoch, M.-H. Whangbo, and R. Kremer, *Z. Anorg. Allgem. Chem.* **636**, 54 (2010).
- <sup>46</sup> M. Hase, K. Ozawa, and N. Shinya, *Phys. Rev. B* **68**, 214421 (2003).
- <sup>47</sup> M. Hase, N. Terada, H. S. Suzuki, H. Kitazawa, K. Ozawa, K. Kaneko, N. Metoki, M. Matsuda, and K. Kakurai, *J. Phys.: Conf. Ser.* **150**, 042051 (2009).
- <sup>48</sup> G. Castilla, S. Chakravarty, and V. J. Emery, *Phys. Rev. Lett.* **75**, 1823 (1995).
- <sup>49</sup> M. Schmitt et al., to be published.
- <sup>50</sup> J. Richter, J. Schulenburg, and A. Honecker, in *Quantum magnetism* (Springer, 2004) Chap. 2, pp. 85–153.
- <sup>51</sup> L. Siurakshina, D. Ihle, and R. Hayn, *Phys. Rev. B* **61**, 14601 (2000).
- <sup>52</sup> R. Nath, A. Tsirlin, E. Kaul, M. Baenitz, N. Büttgen, C. Geibel, and H. Rosner, *Phys. Rev. B* **78**, 024418 (2008).
- <sup>53</sup> U. Löw, *Condens. Matter Phys.* **12**, 497 (2009).